Measured Effects of a Narrowband Interference Suppressor on GPS Receivers

P. T. Capozza, B. J. Holland, T. M. Hopkinson, C. Li, D. Moulin, P. Pacheco, R. Rifkin
ION Annual Meeting
June 1999

ABSTRACT

Narrowband and partial-band interference can severely degrade the performance of GPS receivers. The use of digital signal processing in a receiver has been shown to provide protection against this type of interference in communications systems and has been proposed for application in future GPS systems. This paper discusses the measured effects of narrowband interference suppression on GPS receiver performance. Emphasis is placed on its effects on pseudorange measurements, since navigation accuracy is ultimately the measure of interest to the user. Performance metrics presented include: the GPS receiver input carrier-to-noise ratio, receiver cross-correlation function, and pseudorange errors. The results demonstrate that substantial interference suppression can be attained with modest navigation accuracy degradation by incorporating narrowband interference suppression technology into GPS receivers.

INTRODUCTION

Narrowband and partial-band interference can severely degrade the performance of GPS receivers. When multiple antennas are available to the receiver, their outputs can be combined to effectively reject narrow and/or broadband interference. When only a single antenna is available, as in a hand-held receiver, the receiver's processing gain against narrowband interference may be insufficient. Under these conditions the receiver could use additional signal processing to filter the interference before the satellite range estimates are made. This paper describes the design and performance of one such signal processing technology.

The narrowband interference suppressor technology described in this paper is based on frequency domain excision. The technology is embodied in a 1.5 million-transistor VLSI chip that can either be embedded into a new receiver design or used in an appliqué for use with off-the-shelf legacy GPS receivers. The latter approach has been chosen for this work. Because excision is performed at baseband using 12-bit in-phase and quadrature digital samples, the interference processor in the appliqué implementation is preceded by a high dynamic range RF-to-baseband translator. Processed GPS signals are modulated back to RF by a baseband-to-RF translator. This paper reports performance results using this appliqué with a commercial GPS receiver.

The paper is organized as follows. Section 2 provides an overview of the interference suppressor technology and describes the experimental setup used for testing. Section 3 describes experimental results on the interference suppression capabilities of the appliqué and its effects on GPS receiver performance. Sections 4 and 5 summarize the key conclusions of this study.

HARDWARE

Interference Suppressor Technology

Figure 1 shows a diagram of the appliqué, which includes a custom VLSI chip for performing the interference excision. The frequency domain interference suppression (FDIS) chip contains a 256-point fast Fourier transform (FFT) with provision for amplitude weighting (windowing), a suppression algorithm implementation, and 256-point inverse FFT[1].

The interference suppression algorithm performs a real-time adaptive thresholding implementation that is extremely effective in a changing interference environment. The n th forward FFT output sample for each block of N samples, $X(n), n = 0,1,\ldots, N-1$, is given by:

$$X(n) = \sum_{k=0}^{N-1} w(k)s(k)\, e^{-2pikn/N}, \qquad (1)$$

where $w(k)$ and $s(k)$, $k = 0,1,\ldots, N-1$, are the window coefficients and input signal samples, respectively. The frequency resolution for excision depends on both the sampling rate and N. The maximum complex sampling

rate of the interference suppression chip is 16 million samples per second (MSPS).

A threshold is set for each transform block according to the sample mean and standard deviation of the quantities $\log\left(\left|X(n)\right|^2\right)$ in the frequency domain. This threshold is approximately proportional to the mean noise power without interference. Those frequency bins, ($X(n)$), whose magnitude-square values are greater than this threshold are set to zero, while those below the threshold remain unchanged.

The threshold is set to reduce the interference power as much as possible while minimizing GPS signal degradation. The windowing helps by reducing the inherent frequency broadening of each interferer caused by the finite duration of the FFT. This reduction in the number of frequency samples occupied by a narrowband interferer results in a reduction in the amount of signal energy removed by the excision process. Unfortunately, windowing also degrades carrier-to-noise power spectral density ratio (C/N_0) of the correlator by the factor

$$\frac{\left(\sum_{k=0}^{N-1} w(k)\right)^2}{N\sum_{k=0}^{N-1} w^2(k)},$$

which can be as high as 3dB for the more powerful window functions [2]. For this reason, a second FFT and suppression algorithm runs in parallel with the first with 50% overlap at the inverse FFT output. The overlap allows the "tails" of the window to be eliminated, substantially reducing (but not eliminating) the output C/N_0 loss. The $N/4$ samples at the beginning and end of each inverse FFT block are discarded, leaving the middle $N/2$ samples, which are appended to the $N/2$ samples from the second inverse FFT. Table 1 shows the residual loss for three window functions with 50% overlap. These losses may be included as part of the receiver noise figure budget, since they represent degradation of the output C/N_0. However, the noise figure of a receiver represents added noise, while the losses in Table 1 result from the different power out for the weighted coherent GPS signal as compared to the weighted incoherent noise. An optimal receiver implementation would include an interference detection circuit that would enable the interference suppression only when it is needed. This would reduce insertion loss (and receiver power requirements) in a benign environment.

Table 1. C/N_0 Loss with Windowing and 50% Overlap

Window	C/N_0 Loss (dB)	Sidelobe Level (dB)
Hamming	0.1	41
Kaiser ($b = 7$)	0.2	70
Blackman-Harris (4-term)	0.6	92

Appliqué Configuration

As shown in Figure 1, the appliqué configuration consists of an analog frequency down-converter, the FDIS chip, and an analog frequency up-converter [3]. The appliqué has a gain of 19 dB and a noise figure of 2.7 dB, including the 0.6 dB loss due to the Blackman-Harris window (Table 1). Hence, with no interference, the noise figure would be improved by 0.6 dB in a receiver designed with an enable/disable capability for interference suppression. In all the experiments reported in this paper the 0.6 dB loss is included. The appliqué is linear up to interference levels of 95 dB (single CW) above the GPS signal.

The appliqué has a programmable bandwidth (and complex sample rate) that can be tailored to process different GPS waveforms (C/A code, P-code, or M-code). For the results presented in this paper, the complex sampling rate of the interference suppression appliqué is set at 8.125 MSPS. Hence, the Nyquist bandwidth is 8.125 MHz, yielding an excisor frequency resolution of 32 kHz (8.125 MHz / 256). A CW interferer after windowing and FFT processing occupies approximately 6 frequency bins. Excision of this interference removes roughly 190 kHz of the GPS signal.

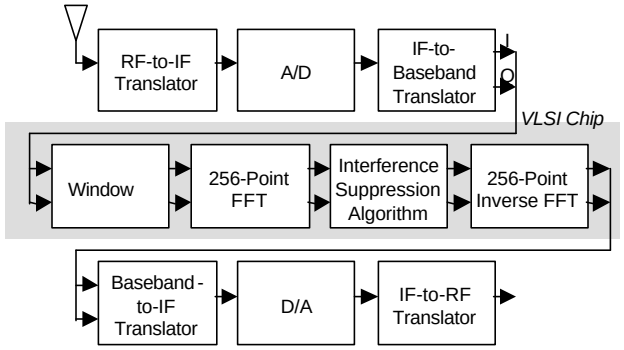

Figure 1. Block Diagram of Appliqué Configuration

Experimental Setup

As shown in Figure 2, the appliqué RF output is connected to the RF input of a commercial GPS receiver. The GPS receiver is a Novatel 3951-R—a wide-bandwidth, 12-channel, C/A-code receiver on a PC card. It has a narrow correlator spacing and 20 s carrier code smoothing. The receiver provides an estimate of the measured C/N_0 at the receiver input as well as an estimate of its position.

The Nyquist bandwidth (8.125 MHz) used for these tests was selected to be approximately four times the C/A-code signal null-to-null mainlobe width (2.046 MHz). Because of anti-aliasing requirements in the receiver front end, the effective 2-dB bandwidth of the appliqué is 80% of the Nyquist bandwidth, or 6.5 MHz. The effective noise figure of the appliqué/GPS receiver combination is 2.8 dB.

The appliqué/receiver combination is tested using the setup diagrammed in Figure 2 [4]. A Nortel GPS satellite simulator generates the satellite signals. The RF power level of these signals is set at –126 dBm (4 dB over the minimum signal specified in GPS ICD-200, but characteristic of the current constellation). Figure 2 shows that the simulated C/A code C/N_0 at the appliqué input is 45 dB-Hz. The Novatel receiver reports estimated C/N_0 of 42.2 dB-Hz, consistent with the noise figure budget. A programmable signal generator provides one or more narrowband interferers, each at a pre-selected power level. The total interference power level varies from -108 dBm to -56 dBm and the interference-to-signal ratio (ISR) varies from 18 to 70 dB. Alternatively, the appliqué's IF output can be captured using a data recording system. The data can then be processed offline to examine the cross-correlation function of the received data with the reference C/A signal.

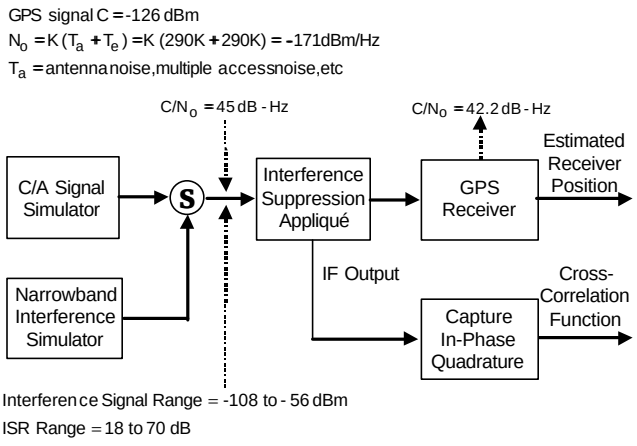

Figure 2. Experimental Setup for Measuring, Cross-Correlation, C/N_0 and Pseudorange Error

EXPERIMENTS

Static Cross-Correlation Measurements

For these experiments the satellite simulator represents a single satellite with vanishing Doppler shift. The IF signal out of the appliqué is captured by a Celerity Data Acquisition system, which records 10-bit samples at a 100 MHz sampling rate. Offline processing consists of converting the samples to complex baseband, bandpass filtering, and cross-correlating with the reference C/A code used on transmit.

Figure 3 shows the cross-correlation function, normalized to unity, for several interference scenarios. The C/A signal power is set to obtain an output C/N_0 of 42.2 dB-Hz. over 10 ms integration time. For this test, the ISR is set at 70 dB. Four scenarios are examined: no interference, one CW interferer at the band center, one CW 125 kHz from band center, and one CW at 300 kHz from band center. The interference is seen to have little effect on the fundamental shape of the cross-correlation function. The precise frequency location of the interference is also seen to have little effect on the main-lobe of the cross-correlation function. The adjacent sidelobes are slightly larger with interference present and reduce as the interference moves away from band center. This suggests that acquisition performance will be affected and that this effect is related to the frequency of the interferer.

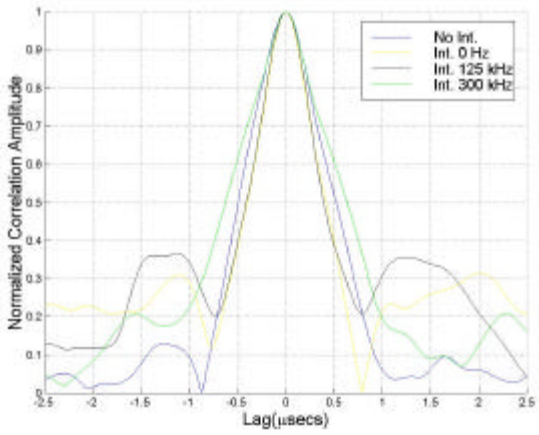

Figure 3. Cross-Correlation Measurements, With and Without a Single CW Interference

Dynamic Pseudorange Error Measurements

In these experiments, the Nortel GPS satellite simulator generates six satellite signals with added Doppler shifts. The satellite simulator is programmed to simulate a receiver that is repetitively executing a commercial airline precision approach pattern [5].

The Novatel receiver can record time-tagged position information and the estimated C/N_0. While estimated C/N_0 is a useful performance measure, the parameter of interest from a user/application perspective is navigation accuracy. One objective is to measure the additional user equipment error (UEE) induced by the insertion of the interference suppressor.

The error in the GPS solution in the simulation set up is the product of the pseudorange error and the vertical dilution of precision (VDOP). Since the geometry factor is known by design, the pseudorange error is estimated by dividing the measured position error by VDOP, which varies with simulation time.

The pseudorange error is obtained by subtracting the GPS receiver's position estimate without interference from that estimated with interference indicated as s^2_{raw}. The pseudorange error due to the receiver, s_{receiver}, is obtained from:

$$s_{\text{receiver}} = \sqrt{s^2_{\text{raw}} - s^2_{\text{baseline}}}$$

where s^2_{baseline} is the error variance without interference. The variance of the collected data (i.e., pseudorange error curve in Figure 4) is obtained by subtracting two independent sets of position measurements without interference. This yields a zero-mean random process whose variance is divided by two to yield s^2_{baseline}. By using this differential measurement technique, the only UEE source is the receiver noise and the loss due to the interference suppressor.

The scenarios investigated are shown in Table 2. The interfering scenarios are grouped into three rather arbitrarily defined classes—benign (one CW tone), moderate (three CW tones), stressful (twenty CW tones). The single-tone scenario frequency is centered in the middle of the C/A code, the three-tone scenario frequencies are uniformly distributed within the null-to-null bandwidth (2 MHz) of the C/A code, and the twenty-tone scenario frequencies are uniformly distributed within the Nyquist bandwidth (8.125 MHz).

The maximum interfering power used is limited by the SNR of the interfering signal source, not the appliqué. While only one realization of each scenario is performed, experience shows that the results are representative. The interference power increases in 2 dB steps every 2 minutes. Over the 52 minute simulation time the total interference power increases 52 dB.

Table 2. Simulation Scenarios

Scenario Type	# CW Interferers	Excision Status
1 Reference	0	Not Engaged
2 Reference	1	Not Engaged
3 Benign	1	Engaged
4 Moderate	3	Engaged
5 Stressful	20	Engaged

Scenario 1 (Reference Run). This test establishes a baseline to measure the relative pseudorange error degradation due to interference with and without the interference suppressor. Figure 4 shows the receiver C/N_0 as reported by the receiver and the pseudorange error for the scenario without interference. Six C/N_0 curves are shown—one for each satellite. The average C/N_0 for the six satellites is 42.2 dB and the s_{raw} (over the scenario timeline) for the reference run is 0.12 meters (i.e., $s_{\text{baseline}} = 0.12/\sqrt{2} \approx 0.09$ m). Not readily visible on the graph about 42 minutes into the scenario, a tracked satellite is lost while a new one is being acquired.

Scenario 2 (Reference with Interference). This test establishes the ISR immunity of the appliqué/receiver without the narrowband interference suppressor being engaged. The C/N_0 for some of the satellites in Figure 5 sometimes decreases dramatically and then recovers. A possible explanation for this is the following. The C/A code spectrum consists of a series of peaks separated by 1 kHz caused by the periodicity of the C/A code. Whenever the interference signal is aligned in frequency with one of the Doppler-shifted peaks, the output C/N_0 is severely degraded. The receiver loses lock (C/N_0 curve) on the six satellites when the ISR is approximately 30 dB (i.e., when the interference power is about 4 dB above the receiver thermal noise power). Even though the receiver has a 30 dB ISR resistance to interference, the pseudorange error over that range increased by 70% over the reference run with no interference (Figure 4).

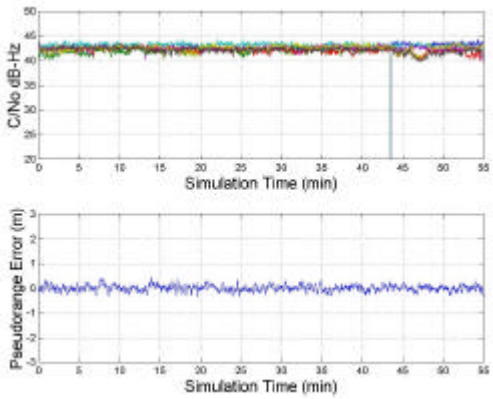

Figure 4. C/N_0 and Pseudorange Error Measurements, No Interference, Interference Suppressor Not Engage

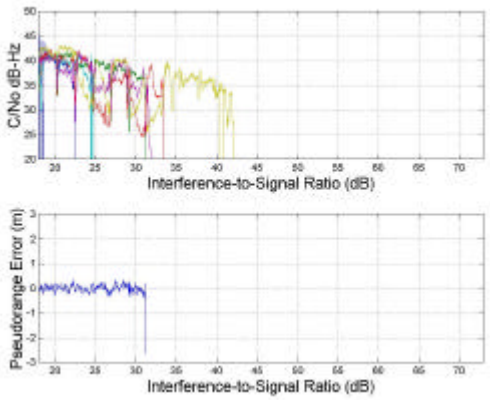

Figure 5. C/N_0 and Pseudorange Error Measurements, Single CW, Interference Suppressor Not Engaged

Scenario 3 (Benign Intereference). This test establishes performance in a benign interference environment. Figure 6 (C/N_0 curve) shows the interference resistance improvement when the interference excision is engaged. The receiver maintains track on the 6 satellites up to 70 dB ISR, the dynamic range limit of the laboratory interference generator. As shown, the C/N_0 curve shows no degradation as the ISR increases. Increasing the ISR has relatively little effect on C/N_0 since the number of frequency domain cells being excised remains approximately constant.

Qualitative examination of Figure 6 shows that the variance of the pseudorange error does not depend on the power of the interference. For ISR below 30 dB the appliqué already provides some benefit against narrowband interference since the pseudorange error over the entire simulation run only increases 50%. This is because of the coherent gain of CW signals in the FFT, interference power is identified and excised well below (– 12 dB) the thermal noise power of the receiver, before it can decrease the C/N_0 . Note that the receiver is able to acquire the new satellite that comes into view when the ISR is about 63 dB.

Scenario 4 (Moderate Interference). This scenario might represent a moderate interfering environment. Results for C/N_0 are shown in Figure 7 and are somewhat worse than those with a single interferer, presumably because there is a higher probability of one of the three interferers aligning with one of the Doppler-shifted peaks in the C/A code's spectrum. Again, the new satellite is acquired under a much more stressful condition.

Scenario 5 (Stressful Interference). This scenario simulates a perhaps-unlikely interfering scenario, but is included to study the robustness of the technology and demonstrate indirectly the immunity to partial band interference. Figure 8 shows results for 20 interferers. While the performance is much better

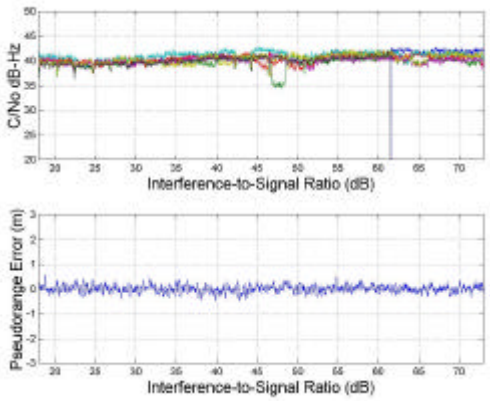

Figure 6. C/N_0 and Pseudorange Error Measurements, Single CW, Interference Suppressor Engaged

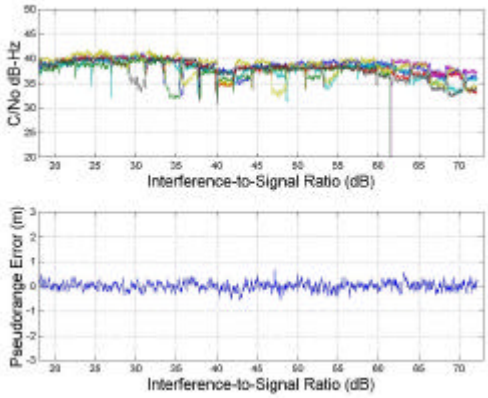

Figure 7. C/N_0 and Pseudorange Error Measurements, Three CWs, Interference Suppressor Engaged

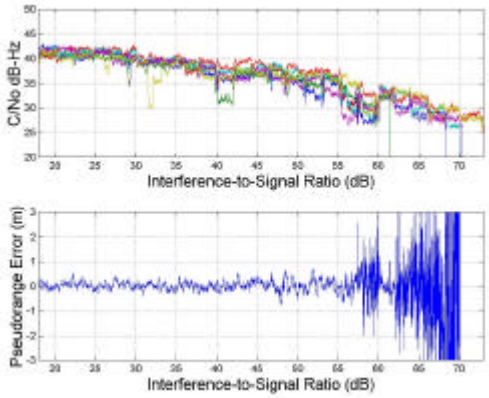

Figure 8. C/N_0 and Pseudorange Error Measurements,Twenty CWs, Interference Suppressor Engaged

than with no excision, it is, as expected, worse than with one or three interferers. This occurs for two reasons: first, some interference power remains unexcised and second, additional GPS signal is being excised along with the interference. Owing to the large number of interferers, even small imperfections in the excision algorithm can leave relatively large residues of unexcised interference energy. With 20 interferers, ~87 bins out of 256 are being excised, which corresponds to 34% of the Nyquist bandwidth.

Figure 8 also shows that the pseudorange error increases with the interference power. For ISR below 54 dB the percentage increase in the pseudorange error is 80%. Above 54 dB ISR the increased pseudorange error reflects the reduced C/N_0 for each satellite. Two satellites are lost when the ISR exceeds 68 dB and the satellite that was acquired 42 minutes into the simulation in the earlier scenarios is not acquired here.

SUMMARY

Against a single CW interferer, the receiver without a narrowband interference suppressor exhibits a 70% increase in pseudorange error up to an ISR of 30 dB. When the interference suppressor is engaged, the receiver exhibits a 50% increase in pseudorange error up to an ISR of 70 dB. This demonstrated improvement against larger ISR (coupled with reduced pseudorange error) is currently limited by test equipment—by design, the appliqué supports 95 dB ISR. Moreover, the interfering power can occupy a large aggregate of the receiver bandwidth (up to 34% has been demonstrated). Therefore, the technology is not limited to narrowband CWs and is suitable to mitigate partial-band interference. The penalty (the importance of which depends on the application) introduced by the technology is quantified by the pseudorange error degradation summarized in Table 3. Under most realistic narrowband interfering scenarios, the relative pseudorange error does not increase by more than 80%. Moreover, the pseudorange error due to receiver noise alone is very small. Hence, increasing the receiver error by 80% might not be significant when other error sources are included in the UEE budget.

If the percentage increase is deemed too large, the results in Table 3 can be used to trade off the receiver noise figure (i.e., cost) for interference immunity. The increased pseudorange error due to the insertion of the narrowband interference suppressor can be viewed as an increase in the receiver noise figure. For example, it was determined experimentally that lowering the noise figure of the appliqué from 2.8 dB to 1.0 dB reduces the pseudorange error by 12%. Therefore, the penalty of using narrowband interference suppressors can be mitigated by designing very low noise figure receivers or appliqués, at higher cost.

Table 3. Percentage of Bandwidth Excised and Relative Pseudorange Errors

Scenario Type	Band Excised %	Raw Error σ_{raw} (m)	Rec. Error $\sigma_{receiver}$ (m)	Rel. Error $\frac{\sigma_{receiver}}{\sigma_{baseline}}$
Baseline	0	0.12	0.09	1.0
1 CW	3	0.15	0.12	1.5
3 CWs	7	0.16	0.14	1.6
20 CWs	34	0.18*	0.15	1.8

* Up to 54 dB ISR

CONCLUSIONS

This paper has demonstrated through measurements the substantial interference immunity improvement of GPS receivers that incorporate narrowband interference suppressor technology and has quantified its effects on GPS position accuracy. The technology presented is generic and can be applied to C/A, P, or M-code receivers. The current VLSI implementation of interference suppression is limited to GPS receivers that have less than 13 MHz bandwidth. A next generation implementation (under development) will take advantage of more advanced VLSI technology to increase useable bandwidths up to 24 MHz and will incorporate design features to reduce power consumption.

ACKNOWLEDGMENTS

This work was funded by the GPS Joint Program Office.

REFERENCES

[1] Capozza, P. T., Holland, B. J., Hopkinson, T. M., Landrau, R. L., "A Single-Chip Narrowband Frequency Domain Excisor for Global Positioning System (GPS) Receiver," Custom Integrated Circuits Conference, May 16-19, 1999, San Diego, CA.

[2] Harris, F. J., "On the Use of Windows for Harmonic Analysis with the Discrete Fourier Transform'' Proceedings of the IEEE, Vol. 66, No. 1, January 1978.

[3] Moulin, D., Solomon, M. N., Hopkinson, T. M., Capozza, P. T., Psilos, J., "High-Performance RF-to-Digital Translators for GPS Anti-Jam Application," Proceedings of the 11th International Technical Meeting of the Satellite Division of the Institution of Navigation, September 15-18, Nashville, Tennessee.

[4] Capozza, P. T., Holland, B. J., Hopkinson, T. M., Moulin, D., Solomon, M., "A Test Facility For Evaluating GPS Anti-Jam Techniques," Proceedings of 1999 National Technical Meeting and 19th Biennial Guidance Test Symposium, January 25-27 1999, San Diego CA.

[5] Leva, J. L., Pacheco, P., "GPS C/A-Code Interference Tests with Proposed Lm Waveforms," Proceedings of the 11th International Technical Meeting of the Satellite Division of the Institution of Navigation, September 15-18, Nashville, Tennessee.